euspen's 25th International Conference & Exhibition, Zaragoza, ES, June 2025
www.euspen.eu

Three-beam constant-force flexure-based translation stage

Loïc Tissot-Daguette[1], Florent Cosandier[1] and Simon Henein[1]

[1]*Instant-Lab, EPFL, Switzerland*

loic.tissot-daguette@epfl.ch

Abstract
Flexure-based constant-force mechanisms belong to the category of zero-stiffness mechanisms. They present a non-zero elastic restoring force which does not depend on the deformation of the mechanism. However, their design and modeling are frequently complex, and most of known designs involve sophisticated and often cumbersome structures, some requiring preloading elements, which restricts their application fields. Furthermore, in most implementations, only a limited region of the force-displacement characteristics provides a constant elastic restoring force. This paper presents a novel constant-force planar flexure-based translation stage consisting of only two parallel beams used to guide the stage, plus an initially straight inclined buckling beam. This additional beam buckles when a compressive critical force is exerted, generating in turn a force offset and a constant negative stiffness along the stage motion direction. For specific design conditions, this negative stiffness can advantageously compensate the intrinsic positive stiffness of the guiding beams. Analytical modeling is conducted based on Euler-Bernoulli beam theory to provide design criteria to make the force constant irrespective of the stage displacement. To validate the analytical modeling and the constant-force behavior, finite element modeling is carried out, as well as experiments on a mesoscale prototype. The mockup is based on three metal blades assembled with 3D-printed plastic parts with an outer volume of 70 x 100 x 6 mm^3. Measurements show that the actuation force is bounded within 10% from a constant-force reference of 1 N for a displacement range of 10 mm. The pre-buckling (compression) region corresponds to only 0.5 mm of travel from the neutral position. Given the unprecedent performances, the compactness and the simplicity of the mechanism, we can conclude that this mechanism constitutes a key building block which could easily be integrated in sophisticated devices such as, force-limiting end-effectors, gravity and stiffness compensation systems, or probes used to passively apply a predetermined contact force onto objects.

Flexures, Constant-force mechanisms, Zero-stiffness mechanisms, Beam buckling

1. Introduction

Compliant constant-force mechanisms (CCFMs) have found applications in various domains, such as overload protection robotic end-effectors [1], biomedical devices [2], and micromanipulation [3]. As opposed to traditional force control methods (e.g., sensor-based control-loop electronic systems), CCFMs passively apply a nearly constant force over a specific deflection range.

The majority of CCFM architectures combine the negative stiffness of a bistable mechanism (usually relying on buckling members) and the inherent positive stiffness of flexures to generate a constant-force output [4]. CCFMs can also rely on beams with complex pre-curvatures. This kind of design requires compatible manufacturing technologies (e.g., 3D-printing, electrical discharge machining or deep reactive ion etching) and shape optimization processes [1,4]. Nevertheless, the output force of most CCFMs is only constant within a limited stroke. Moreover, they are cumbersome, are difficult to design and have a low support stiffness since they often lack guiding elements.

This paper presents a novel CCFM which is primarily based on an inclined initially straight beam that buckles to provide in turn a constant force when the mechanism is deflected. Two additional parallel beams are integrated to efficiently guide the moving stage in translation as well as to compensate the negative stiffness of the inclined beam. The presented mechanism is described, analytically modeled and designed in Secs. 2, 3 and 4, respectively. Its constant-force behavior is validated using finite element modeling in Sec. 5 and experimentally in Sec. 6. Section 7 presents the results of this study along with potential applications of the mechanism. Finally, concluding remarks are provided in Sec. 8.

2. Mechanism description

The new Constant-Force Translation Stage (CFTS) planar mechanism (Fig. 1) consists of two parallel guiding beams supporting a moving block in translation, plus an inclined initially straight buckling beam that buckles when a critical level of actuation force F_{in} is reached.

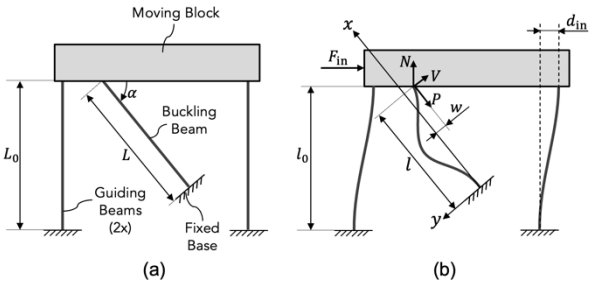

Figure 1. Constant-Force Translation Stage (CFTS) in (a) neutral and (b) deflected positions. Note that N, V and P are internal forces.

The deformed shaped of the inclined beam corresponds to that of a fixed-guided buckled beam. It exerts a constant axial force and a lateral constant negative stiffness onto the moving block [5,6]. For specific dimensions of the mechanism, this negative stiffness can be used to compensate the positive

stiffness of the two guiding beams. Advantageously, the actuation force F_{in} can thus be made constant irrespective of the displacement d_{in}. The mechanism may be conveniently manufactured in a monolithic form and has the benefit of being planar and compact. Moreover, the inclined buckling beam which is in parallel to the two guiding beams provide additional support stiffness to the CFTS. Note that the inclined beam can buckle in either direction without modifying the force-displacement characteristics of the stage. Depending on the application requirements (size, constant-force value and range of motion), the buckling beam could be placed on the opposite side of the moving block (i.e., $\alpha < 0$ in Fig. 1), as discussed in Sec. 3.2.

3. Analytical model

This section introduces the analytical model used to design the CFTS illustrated in Fig. 1. For the calculations, we assume that all the beams are slender and initially straight. The flexural rigidities of the buckling beam and the guiding beams are respectively EI and EI_0, considered constant along their respective beam lengths L and L_0. We also assume that the out-of-plane thickness b of the mechanism is sufficiently large to avoid any out-of-plane motion of the moving block. The stiffness of the guiding beams is sufficient to withstand the reaction moment applied by the buckling beam to the moving block. The stage displacement d_{in} is small enough for the material to stay in its elastic domain and to satisfy the small-deformation assumption of beams. Furthermore, gravity and dynamics are neglected.

3.1. Force-displacement relationship

The equilibrium of the internal and external forces leads to:

$$N = P\sin(\alpha) - V\cos(\alpha) \tag{1}$$

and:

$$F_{\text{in}} = K_0 d_{\text{in}} + P\cos(\alpha) + V\sin(\alpha) \tag{2}$$

where K_0 is the stiffness of the two guiding beams which is equal to the stiffness of a so-called parallel spring stage. This stiffness is function of the load N applied perpendicularly to the stage following the formula given by [7] as:

$$K_0 = \frac{24EI_0}{L_0^3}\left(1 + \frac{L_0^2 N}{2\pi^2 EI_0}\right) \tag{3}$$

The deflection of the inclined beam corresponds to a fixed-guided buckling configuration. Considering that this beam is in second mode branch, its compression is constant and equal to $P = 4\pi^2 EI/L^2$ and its laterally applied force is negative and linear with respect to its lateral displacement following $V = -4\pi^2 EI/L^3 \cdot w$ [5,6]. The actuation force F_{in} can then be linearized by substituting the approximate displacement relationship $w \cong d_{\text{in}}\sin(\alpha)$ in Eqs. (1) to (3):

$$F_{\text{in}} \cong F_{\text{cst}} + K_{\text{tot}}\, d_{\text{in}} \tag{4}$$

where:

$$F_{\text{cst}} = \frac{4\pi^2 EI}{L^2}\cos(\alpha) \tag{5}$$

and:

$$K_{\text{tot}} = \frac{24EI_0}{L_0^3} + \frac{48EI}{L_0 L^2}\sin(\alpha) - \frac{4\pi^2 EI}{L^3}\sin^2(\alpha) \tag{6}$$

The input force can therefore be approximately constant (i.e., $F_{\text{in}} \cong F_{\text{cst}}$) if $K_{\text{tot}} = 0$, see Eq. (4).

3.2. Translational stroke

The stroke of the translation stage is either limited by the material yielding or by the loss of preloading of the buckling beam. In the first case, classical flexure design methods can be utilized to compute the admissible strain of the guiding and buckling beams [7,8]. For the second case, the mechanism range of motion corresponds to the stroke of the buckling beam where its lateral stiffness remains constant and negative. From [5], the following inequality must be respected:

$$\Delta l \geq \frac{3}{4}\frac{w^2}{L} \tag{7}$$

where $\Delta l = L - l$ is the preload displacement of the buckling beam which is related to the input displacement d_{in} as follows:

$$\Delta l = d_{\text{in}}\cos(\alpha) + \lambda_0\sin(\alpha) \tag{8}$$

where $\lambda_0 = L_0 - l_0 \cong 3/5 \cdot d_{\text{in}}^2/L_0$ is the parasitic shift of the moving block [7]. Then from Eqs. (7) and (8), the maximum stroke is given by:

$$d_{\text{in,max}} = \frac{\cot(\alpha)}{\frac{3}{4}\frac{L_0}{L}\sin(\alpha) - \frac{3}{5}}L_0 \tag{9}$$

As can be seen in Eq. (9), the condition $L_0/L \cdot \sin(\alpha) > 4/5$ must always be satisfied for the proper functioning of the constant-force mechanism. Thus, the inclination α must be sufficiently high for a given length ratio L_0/L. However, it should be noted that when α approaches 90°, the stroke $d_{\text{in,max}}$ (Eq. (9)) and the constant-force value F_{cst} (Eq. (5)) decrease. Therefore, ideal values of α and L_0/L need to be determined based on application requirements.

Note that the buckling beam can alternatively be placed on the opposite side (i.e., $\alpha < 0$). However, the mechanism stroke $d_{\text{in,max}}$ would be comparatively reduced since the guiding beam parasitic shift λ_0 is oriented in opposition to the buckling beam preloading displacement Δl. Despite this, the condition $K_{\text{tot}} = 0$ (Eq. (6)) can be then attained for a reduced length ratio L_0/L when fixed flexural rigidities EI and EI_0 are considered, which may lead to a smaller mechanism size.

4. Design

In this section, a flexure-based mesoscale mockup of the CFTS, aiming for a translation stroke of 10 mm and a constant-force value of 1 N is designed. All three beams are made of spring strips with thickness $h = h_0 = 0.1$ mm and width $b =$ 6 mm. The beam material (stainless steel 1.4310) is selected for its high yield strength σ_y (approximately 1400 MPa). As illustrated in Fig. 2, all the beams are clamped to the moving block and to the fixed base, which are 3D printed using conventional Fused Deposition Modeling (FDM) and PLA filament.

Based on the analytical model (Sec. 3), we first select a buckling beam inclination of $\alpha = 60°$ in order to obtain a relatively large stroke $d_{\text{in,max}}$. The beam lengths L and L_0 are respectively computed using Eqs. (5) and (6) by substituting $F_{\text{cst}} = 1$ N and $K_{\text{tot}} = 0$. Finally, the guiding beams are separated by a distance $D_0 = 60$ mm to ensure a relatively

high support stiffness of the moving block. The parameter values are reported in table 1.

The theoretical stroke given by Eq. (9) leads to $d_{\text{in,max}} = 87.5$ mm. Since this value is bigger than the guiding beam length, we can assume that yielding will be the first factor limiting the range of motion of the mechanism. In the experiment (Sec. 6), the stroke is limited to 10 mm corresponding to a simulated von Mises stress of 940 MPa (Sec. 5) in order to obtain a safety factor of 1.5 with respect to the material yield strength σ_y.

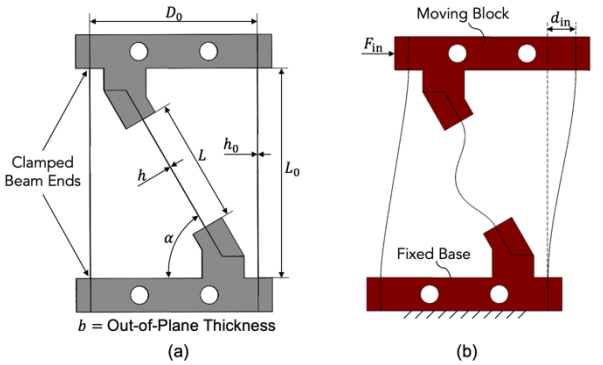

Figure 2. Schematics of the mesoscale prototype of the CFTS shown (a) as-fabricated and (b) deflected

Table 1. Design parameters of the CFTS mechanism

Structure Part	Parameter	Value
Material (stainless steel 1.4310)	E	200 GPa
	σ_y	1400 MPa
Buckling beam	h	0.1 mm
	L	44.5 mm
	α	60°
Guiding beams	h_0	0.1 mm
	L_0	75 mm
	D_0	60 mm

5. FEM Simulation

Finite Element Method (FEM) modeling was carried out to verify the constant-force behavior of the designed CFTS mockup. The commercial software COMSOL Multiphysics 6.1 is employed to conduct a 2D plane stress stationary study. The Geometric Nonlinearity setting is used to capture the large deformation and buckling behaviors of the structure. The beams are all meshed with 4 and 400 quadrilateral solid elements along their thickness and length, respectively.

The force-displacement characteristics of the CFTS is assessed by varying the translation displacement d_{in} of a rigid connector attached to the moving block and evaluating the reaction force F_{in}, while the fixed base is fully constrained. In order to assist the inclined beam in buckling in a given direction, a load is supplied laterally to it at the beginning of the study. This load is subsequently removed to evaluate the effective translation stiffness of the CFTS.

6. Experiment

The CFTS mesoscale prototype designed in Sec. 4 is fabricated and its force-displacement characteristics is experimentally characterized using a dedicated testbench. The testbench consists of a manual micro-positioning stage and a force sensor (Kistler model 9207), to respectively push the moving block by a displacement d_{in} and measure the elastic restoring force F_{in} (Fig. 3). The equipment and the fixed base of the CFTS are rigidly fastened to an optical table. The mechanism plane is perpendicular to the direction of gravity to minimize the risk of detecting forces associated with gravity. The measurements are performed for each increment of the moving block position when the system is static. Five repetitions are used to average the force measurement to minimize sensor noise. The measurement uncertainty is assumed to be ±0.02 N for the actuation force F_{in} and ±0.05 mm for the moving block displacement d_{in}.

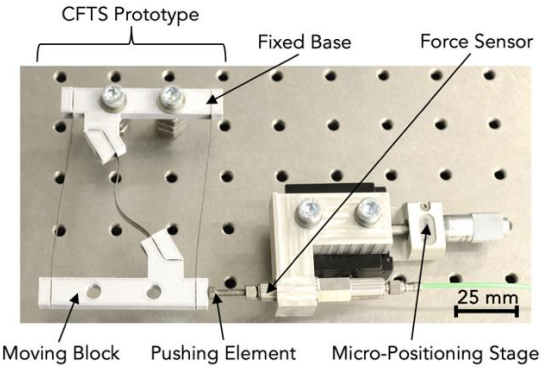

Figure 3. Experimental setup used for the characterization of the CFTS prototype

7. Results and discussion

7.1. Constant-force characteristics

Figure 4 presents the force-displacement characteristics of the CFTS. The analytical model, the FEM model and the experimental data are plotted together to analyze the consistency of the results. The deviation between the analytical and FEM models is bounded within 2%, demonstrating the preciseness of the formulas derived in this paper. The maximum discrepancy between the analytical and experimental results only reaches a 10% relative difference. We may thus infer that all data types are in good agreement.

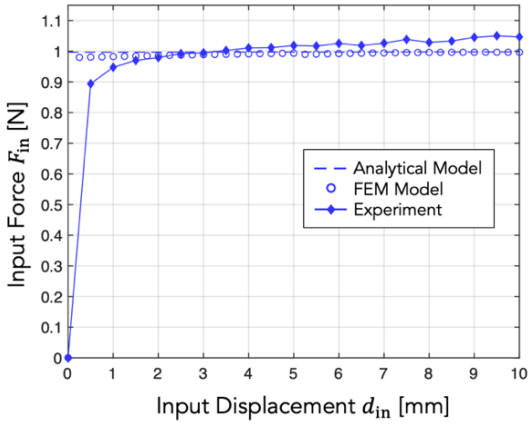

Figure 4. Force-displacement characteristics of the CFTS

The constant-force behavior of the CFTS is demonstrated by the results in Fig. 4. A small tangential stiffness can be observed in the constant-force region of the experimental force-displacement characteristics. This non-zero stiffness constant ($K_{\text{tot}} \neq 0$) is assumed to be due to manufacturing and assembly tolerances leading to errors in the effective dimensions of the beams. The constant-force region is reached after 0.5 mm of travel from the neutral position. This pre-buckling displacement amounts to only 5% of the total stroke of the CFTS (10 mm).

7.2. Potential applications

The CFTS can easily be integrated in more complex flexure-based structures. For instance, the CFTS could be used in passive multi-degree-of-freedom (multi-DOF) force-limiting devices. In a simple arrangement, a two-way constant-force

mechanism can be created by using two CFTS in series, see Fig. 5a. When the moving block is displaced to the left, the buckling beam of the CFTS2 is in tension, whereas the buckling beam of the CFTS1 buckles, thus limiting the applied force to a constant value F_{cst} (Fig. 5b). The same constant-force characteristics applies in the reverse direction (i.e., when the moving block is displaced to the right). In that case, CFTS2 buckles and CFTS1 is in tension (Fig. 5c).

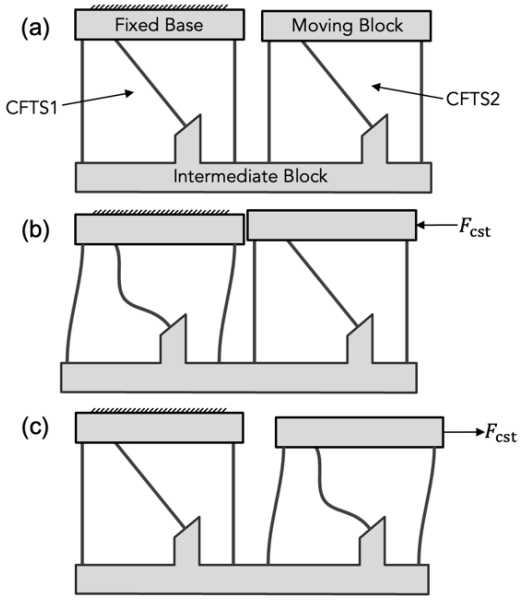

Figure 5. Two-way constant-force translation stage mechanism using two CFTS in series: (a) in neutral position, (b) when displaced to the left and (c) when displaced to the right

In a prior work, we introduced a mechanism based on a flexure pivot preloaded by a spring for stiffness adjustment [9]. It was observed that the pivot stiffness variates with the rotation angle, which is disadvantageous for applications requiring a linear moment-angle characteristics. Figure 6 illustrates a flexure-based implementation of the mechanism presented in [9] but where a CFTS is used instead of a spring. In that case, the flexure pivot is preloaded by a constant force F_{cst} resulting in a constant angular stiffness M_θ/θ [9, Eq. (8)].

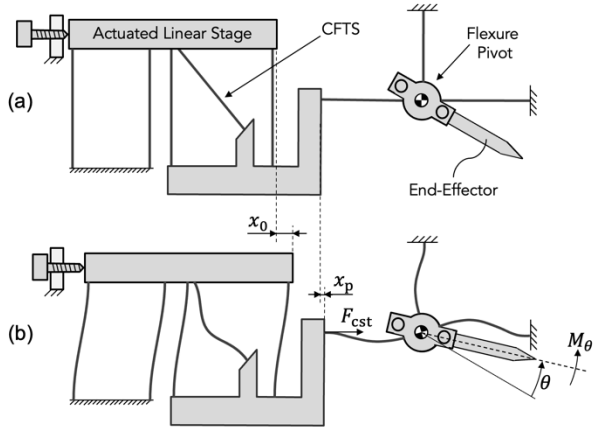

Figure 6. Flexure pivot preloaded by a CFTS: (a) in neutral position and (b) in preloaded and deformed position

Depending on the level of the preload F_{cst}, the stiffness value can be positive (stiffness tuning), near-zero (static balancing) and negative (bistable behavior). Note that the stiffness is only reduced for the angular stroke where the preloading displacement x_0 is bigger than the end-shortening x_{p} of the pivot horizontal beams. Keep in mind that the pivot stiffness is invariant of x_0 and hence cannot be adjusted post fabrication (as opposed to the spring-based design [9]). Potential applications for this new flexure pivot with reduced stiffness include load cells with high sensitivity and high linearity [9] and low-frequency flexure oscillators with minimized isochronism defect [10].

8. Conclusion

This paper presents a new planar flexure translation stage that advantageously exhibits a constant elastic restoring force. The mechanism is designed and optimized in terms of translational stroke and force response using analytical and FEM modeling. A mesoscale mockup of the mechanism with an overall size of 70 x 100 x 6 mm^3 is fabricated and its force-displacement characteristics is measured. The experimental results, which are in good agreement with theoretical models, demonstrate the constant-force behavior of the mechanism. More specifically, the prototype exhibits a restoring force of 1 N that is constant within a 10% margin for a total translational stroke of 10 mm. The pre-buckling travel (i.e., the displacement from the neutral position required to reach the constant-force region) is less than 5% of the total stroke.

This novel mechanism being simple and compact, and efficient in terms of constant-force behavior and pre-buckling travel, has the potential for being integrated in more sophisticated flexure-based mechanisms. Application examples include multi-DOF force-limiting devices, as well as stiffness reduction of load cells and watch oscillators.

References

[1] Lan C, Wang J and Chen Y 2010 A Compliant Constant-Force Mechanism for Adaptive Robot End-Effector Operations *2010 IEEE International Conference on Robotics and Automation Anchorage Convention District* Anchorage, USA

[2] Tissot-Daguette L, Baur C, Bertholds A, Llosas P and Henein S 2021 Design and modelling of a compliant constant-force surgical tool for objective assessment of ossicular chain mobility *21st International Conference on Solid-State Sensors, Actuators and Microsystems (Transducers)* Orlando, USA

[3] Liu Y, Zhang Y and Xu Q 2017 Design and control of a novel compliant constant-force gripper based on buckled fixed-guided beams *IEEE ASME Trans. Mechatron.* **22** 476-486

[4] Wang P and Xu Q 2018 Design and modeling of constant-force mechanisms: A survey *Mech. Mach. Theory* **119** 1-21

[5] Tissot-Daguette L, Schneegans H, Gubler Q, Baur C and Henein H 2022 Rectilinear translation four-bar flexure mechanism based on four Remote Center Compliance pivots *Euspen's 22nd International Conference & Exhibition* Geneva, CH

[6] Tissot-Daguette L, Cosandier F, Gubler Q, Petremand Y, Despont M and Henein S 2025 Residual Stress Chevron Preloading Amplifier for Large-Stroke Stiffness Reduction of Silicon Flexure Mechanisms *J. Micromech. Microeng.* **35** 025003

[7] Henein S 2000 *Conception des structures articulées à guidages flexibles de haute précision* EPFL Ph.D. thesis n°2194.

[8] Tissot-Daguette L, Schneegans H, Thalmann E and Henein S 2022 Analytical modeling and experimental validation of rotationally actuated pinned–pinned and fixed–pinned buckled beam bistable mechanisms *Mech. Mach. Theory* **174** 104874

[9] Tissot-Daguette L, Smreczak M, Baur C and Henein S 2021 Load cell with adjustable stiffness based on a preloaded T-shaped flexure pivot *euspen's 21st International Conference & Exhibition* Copenhagen, DK

[10] Thalmann E 2020 *Flexure Pivot Oscillators for Mechanical Watches* Ph.D. thesis (EPFL)